

Routes to chaos and complete phase locking in modulated relaxation oscillators

Bo Christiansen

*Physics Laboratory, University of Copenhagen, H.C. Ørsted Institute, Universitetsparken 5,
DK-2100 Copenhagen Ø, Denmark*

Preben Alstrøm

*Physics Laboratory, University of Copenhagen, H.C. Ørsted Institute, Universitetsparken 5,
DK-2100 Copenhagen Ø, Denmark
and Center for Polymer Studies, Boston University, 590 Commonwealth Avenue, Boston, Massachusetts 02215*

Mogens T. Levinsen

*Physics Laboratory, University of Copenhagen, H.C. Ørsted Institute, Universitetsparken 5,
DK-2100 Copenhagen Ø, Denmark*

(Received 2 January 1990)

Relaxation oscillations are very commonly found in nature. When modulated by an external field, such systems show phase-locked, quasiperiodic, or chaotic behavior, dependent on the specific parameters. We present an *exact* analysis for a triangular modulated relaxation oscillator and determine the parameter-space phase diagram. We identify critical lines associated with qualitatively different transitions to chaos and complete phase locking (CPL). One transition is related to overlapping of phase-locked regions and is also identified as the transition from quasiperiodicity to chaos described by a noninvertibility of the Poincaré map. Another is a nonchaotic transition to a CPL regime, where a gap appears in the Poincaré map. Also, we find a sudden transition between this CPL regime and a regime where all attractors are chaotic. The critical lines separating the different regimes are found and attributed to either a horizontal or vertical line segment in the Poincaré map. Moreover, we find analytically a number of scaling relations for the phase-locked stability intervals on and nearby the critical lines. We also comment on the situation when the modulation is sinusoidal and when damping is present.

When a nonlinear oscillator is modulated, phase locking may occur between the intrinsic frequency and the frequency of the modulation. For many such systems the general behavior is well captured by the circle map.¹ At small nonlinearity, phase locking is not pronounced, and the complement of the phase-locked regions has a positive measure. On this set the orbits are quasiperiodic. However, increasing the nonlinearity, the phase locking becomes more dominant, and reaching a certain critical line in parameter space, phase locking is encountered almost everywhere—only a set of *zero* measure is left for quasiperiodic orbits. The phase locking is said to be *complete*. Crossing the critical line the phase-locked regions start to overlap and chaos develops. The critical line can be identified by the existence of a horizontal inflection point in the circle map.

In contrast to the *simultaneous* transition to chaos and complete phase locking (CPL) observed in usual circle map systems,¹ recent reports on experiments have given evidence to the existence of oscillating systems showing complete phase locking in entire *nonchaotic* regions.²⁻⁴ In a previous paper,⁵ we have explained the presence of such regions as a consequence of an “integrate-and-fire” phenomenon where a variable V develops continuously in time (integrates) except when it reaches an upper threshold T_{top} , where V is reset to the value of a lower threshold T_{bot} (firing). The integrate-and-fire phenomenon is

not only known from electronic oscillators,⁶ but is generally encountered in a number of physical, chemical, and biological systems with Lorentz-type attractors, where trajectories greatly separate over short times.⁵ Examples include systems as diverse as charge-density-waves systems,⁷ the Belousov-Zhabotinskii reaction,³ and neuronal encoding.⁸

Reference 9 gives a characterization of integrate-and-fire systems varying the exact way of enforcing an external modulation. In particular, it is shown that modulation on the upper threshold gives rise to a *nonchaotic* CPL region. In contrast, a lower threshold modulation yields the usual circle map dynamics, including a transition from quasiperiodicity to chaos. The former is accompanied by a gap, the latter by a noninvertibility of the Poincaré map [i.e., $V_{n+1} = V(t_{n+1})$ as function of $V_n = V(t_n)$, where $t_{n+1} - t_n = T$ and T is the period of the modulation].

In this paper we give an exact description of a simple one-dimensional integrate-and-fire system showing both kinds of supercritical behavior. Such systems found in nature include the self-oscillating Belousov-Zhabotinskii reaction (two competing internal frequencies),³ the externally modulated electronic relaxation oscillator,⁴ and certain combined electronic-optical feedback systems with time delay.¹⁰ While the equations for the electronic relaxation oscillator can be deduced with regards to the

modulation on both levels, the other systems are too complicated, and the information about the level modulation can only be deduced from the actual return maps. For simplicity we choose a linear growth between firings and put a triangular modulation $M(t)$ with equal frequencies and phases but different amplitudes A_{top} and A_{bot} on the thresholds (Fig. 1),

$$\dot{V} = I, \tag{1}$$

$$V(t^+) = A_{bot}M(t) \text{ if } V(t) = 1 + A_{top}M(t), \tag{2}$$

where

$$M(t) = \begin{cases} 4(t - n - \frac{1}{4}) & \text{if } n \leq t \leq n + \frac{1}{2} \\ -4(t - n - \frac{3}{4}) & \text{if } n + \frac{1}{2} \leq t \leq n + 1 \end{cases} \tag{3}$$

(n is an integer). The frequency is set to 1 and the dc values of the thresholds T_{top} and T_{bot} to 1 and 0, respectively. The positive control parameter I with the two amplitudes gives a three-dimensional parameter space (I, A_{bot}, A_{top}) .¹¹ Although these parameters are *independent*, we shall for convenience define the normalized amplitudes $\hat{A}_{bot} = 4A_{bot}/I$ and $\hat{A}_{top} = 4A_{top}/I$. This system of equations does not represent any of the above-mentioned experiments exactly, but it does contain the most important features.

Each phase-locked region is characterized by a constant rational rotation number $R = P/Q$, defined as the average number of firings in one period of the modulation. Figure 1 shows an attractor with $R = \frac{3}{2}$. We define the firing function f by $\tau_1 = f(\tau_0)$, where τ_1 and τ_0 are successive firing times. Since the modulation is piecewise linear with period 1, f is also piecewise linear, fulfilling the circle-map condition $f(t+n) = f(t) + n$. A periodic attractor with rotation number $R = P/Q$ will, after P firings in a time interval Q , close on itself, $V(t+Q) = V(t)$, and

$$f^P(\tau_0) = Q + \tau_0. \tag{4}$$

To determine the stability of the attractor consider the P distinct firings at times $\tau_0, \tau_1, \dots, \tau_{P-1}$. We note that the firings in intervals $[n, n + 1/2]$, where $M(t)$ is increasing, will result in a change of the distance of close trajectories with a factor of

$$\Lambda_- = \frac{1 - \hat{A}_{bot}}{1 - \hat{A}_{top}}. \tag{5}$$

This is apparent from Fig. 2: An initial distance ΔV_1 between nearby trajectories yields a difference in firing time Δt given by

$$I \Delta t = \Delta V_1 + 4 A_{top} \Delta t. \tag{6}$$

The resulting distance ΔV_2 between the trajectories after firing is determined similarly by

$$I \Delta t = \Delta V_2 + 4 A_{bot} \Delta t. \tag{7}$$

Hence $\Lambda_- \equiv \Delta V_2 / \Delta V_1 = (1 - \hat{A}_{bot}) / (1 - \hat{A}_{top})$. Analogously, firings in the intervals $[n + 1/2, n + 1]$ result in a change of the distance between nearby trajectories with a

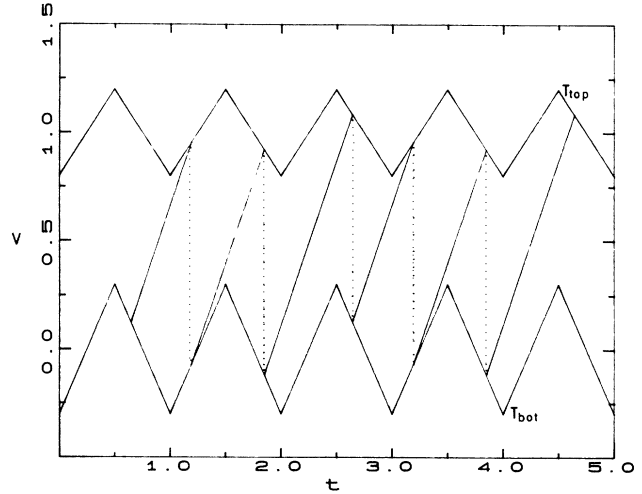


FIG. 1. An attractor on the $\frac{3}{2}$ step for $(I, A_{bot}, A_{top}) = (1.51, 0.3, 0.2)$.

factor of

$$\Lambda_+ = \frac{1 + \hat{A}_{bot}}{1 + \hat{A}_{top}}. \tag{8}$$

Thus, if P_- of the P firings takes place in the intervals $[n, n + 1/2]$, and P_+ firings occur in the intervals $[n + 1/2, n + 1]$, ($P_- + P_+ = P$), the criterion for stability is

$$\Lambda(\tau_0) = |\Lambda_-^{P_-} \Lambda_+^{P_+}| < 1, \tag{9}$$

i.e., the Liapunov exponent $\lambda = \ln \Lambda$ must be negative.

A point in parameter space lies in the P/Q phase-locked region if a τ_0 exists fulfilling both conditions (4) and (9). Keeping the amplitudes A_{bot} and A_{top} fixed and varying I , the upper edge I_u and lower edge $I_l \leq I_u$ of a phase-locked region can be found from where one of these conditions breaks down. The exact way this breakdown occurs depends on the position in parameter space.

The reduced parameter space $(\hat{A}_{bot}, \hat{A}_{top})$ can be divided in several regions characterized by the types of motion allowed (Fig. 3). The regions in the reduced parameter space $(\hat{A}_{bot}, \hat{A}_{top})$, the values of Λ_- and Λ_+ , and the different types of motion are summarized in Table I. We shall see that the critical lines associated with transitions to chaos and CPL depend solely on the normalized amplitudes \hat{A}_{bot} and \hat{A}_{top} . However, the parameter space is three dimensional and only by fixing one parameter (e.g., I), the actual position of the steps in $(\hat{A}_{bot}, \hat{A}_{top})$ space is determined. To illustrate this, some of the phase-locked regions are shown in (I, A_{bot}) space for constant $A_{top} = 0.2$ (Fig. 4) and in (I, A_{top}) space for constant $A_{bot} = 0.2$ (Fig. 5).

Consider first $\hat{A}_{top} > 1$, i.e., the parameters above the line $k_l: \hat{A}_{top} = 1$ where the increasing part of the upper threshold has slope I . In this region the decreasing parts of the modulation shadow the increasing ones and prevent any firings there (Fig. 6). In this region firings

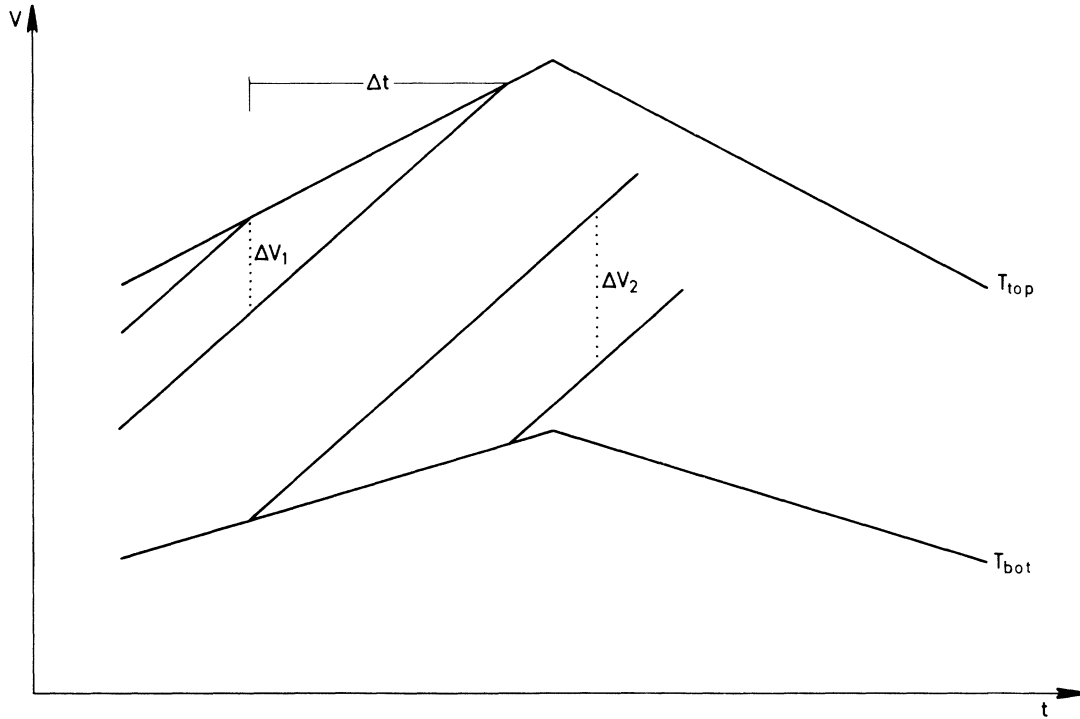


FIG. 2. Trajectories separated by a distance ΔV_1 will, after a firing, be separated by ΔV_2 . Δt is the difference in firing time.

only occur in the intervals $[n + 1/2, n + 1]$, resulting in a Liapunov exponent proportional to $\ln \Lambda_+$ and therefore [Eq. (8)] negative when $\hat{A}_{top} > \hat{A}_{bot}$ (region A) and positive when $\hat{A}_{top} < \hat{A}_{bot}$ (region B). In the former case the attractors are always phase locked and we have CPL in the entire region A.¹² In the latter case all attractors will

be chaotic. Everywhere on the line $l_1: \hat{A}_{top} = \hat{A}_{bot}$, between the regions A and B, both Λ_- and Λ_+ equal 1 and almost all attractors will be quasiperiodic with irrational rotation number R . Since the average increase of V between two successive firings is I/R and each firing decreases V by exactly 1 along the line l_1 , we have $R = I$ on l_1 .

In region A, the firing function f (Fig. 7) consists of line segments with slope Λ_+ and $\Lambda_{*} = (1 - \hat{A}_{bot}) / (1 + \hat{A}_{top})$ and a vertical gap of size $g = \hat{A}_{top} / (1 + \hat{A}_{top})$. The gap is due to the shadowing at the upper modulation. Moreover, since all firings take place on the decreasing part of the upper modulation, all firing times τ_i for an attractor will lie on the intervals where f has slope Λ_+ . The value μ defined by $f(-\mu) = 0$ (Ref. 13) gives a measure of f 's distance to the diagonal (Fig. 7). Outside the $1/Q$ phase-locked regions, μ is a smooth function of the parameters

$$\mu = \frac{1/I - \hat{A}_{top}/4 + \hat{A}_{bot}(K + \frac{1}{4})}{1 + \hat{A}_{bot}}, \quad (10)$$

between $R = 1/K$ and $R = 1/(K + 1)$. Varying μ by changing I while keeping \hat{A}_{top} and \hat{A}_{bot} fixed only changes the distance from f to the diagonal. Under these conditions one can determine the width $\Delta\mu(P/Q)$ of the stability interval for $R = P/Q$ (called the P/Q step below),¹⁴

$$\sum_{m=0}^{P-1} \Lambda_+^m \Delta\mu(P/Q) = \begin{cases} g & \text{if } P=1 \\ (1-g)(1-\Lambda_+)\Lambda_+^{P-2} & \text{if } P>1, \end{cases} \quad (11)$$

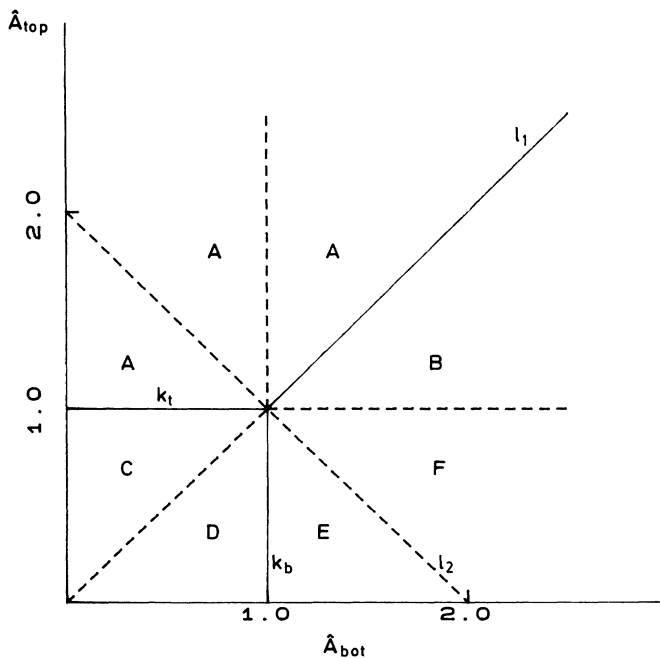


FIG. 3. The lines k_t , k_b , l_1 , and l_2 and the different regions in $(\hat{A}_{bot}, \hat{A}_{top})$ space.

TABLE I. The different regions in parameter space and the type of their solutions.

Region	Λ_-	Λ_+	Motion
<i>A</i>	$\hat{A}_{\text{bot}} < \hat{A}_{\text{top}}, \hat{A}_{\text{top}} > 1$	Forbidden	< 1 Periodic
<i>B</i>	$\hat{A}_{\text{bot}} > \hat{A}_{\text{top}} > 1$	Forbidden	> 1 Chaotic
<i>C</i>	$\hat{A}_{\text{bot}} < 1, \hat{A}_{\text{top}} < 1, \hat{A}_{\text{bot}} < \hat{A}_{\text{top}}$	> 1	< 1 Periodic and quasiperiodic
<i>D</i>	$\hat{A}_{\text{bot}} < 1, \hat{A}_{\text{top}} < 1, \hat{A}_{\text{bot}} > \hat{A}_{\text{top}}$	$> 0, < 1$	> 1 Periodic and quasiperiodic
<i>E</i>	$\hat{A}_{\text{bot}} > 1, \hat{A}_{\text{top}} < 1, \hat{A}_{\text{top}} + \hat{A}_{\text{bot}} < 2$	$< 0, > -1$	> 1 Periodic and chaotic
<i>F</i>	$\hat{A}_{\text{bot}} > 1, \hat{A}_{\text{top}} < 1, \hat{A}_{\text{top}} + \hat{A}_{\text{bot}} > 2$	< -1	> 1 Chaotic

where the right-hand side in Eq. (11) is the size of the gap when iterated $P-1$ times by f . From Eq. (11) we have, for $P > 1$,

$$\Delta\mu(P/Q) = (1-g)(1-\Lambda_+)^2 \frac{\Lambda_+^{P-2}}{1-\Lambda_+^P} \tag{12}$$

Converting from μ to $1/I$ we have $[(1-g)(1+\hat{A}_{\text{bot}})=\Lambda_+]$,

$$\Delta \frac{1}{I}(P/Q) = (1-\Lambda_+)^2 \frac{\Lambda_+^{P-1}}{1-\Lambda_+^P} \tag{13}$$

For the $1/Q$ steps we have $\mu=Q$ for $I=I_l(1/Q)$ ($K=Q$). Hence, by Eq. (10),

$$1/I_l = Q + (\hat{A}_{\text{top}} - \hat{A}_{\text{bot}})/4 \tag{14}$$

Similarly, $\mu=Q-g$ for $I=I_u(1/Q)$ ($K=Q-1$) yields

$$1/I_u = Q - (\frac{3}{4}-g)(\hat{A}_{\text{top}} - \hat{A}_{\text{bot}}) \tag{15}$$

Since $(1-g)(\hat{A}_{\text{top}} - \hat{A}_{\text{bot}}) = 1-\Lambda_+$, Eq. (13) is also valid for $P=1$.

Equation (13) holds in all of the regime *A* including the critical line k_l . From Eq. (13) one can show analytically¹⁴

$$\sum_{1/(K+1) \leq P/Q < 1/K} \Delta \frac{1}{I}(P/Q) = 1 \tag{16}$$

Since also (for fixed \hat{A}_{bot} and \hat{A}_{top})

$$1/I_l[1/(K+1)] - 1/I_l(1/K) = 1 \tag{17}$$

[Eq. (14)], the phase locking is complete—the complement of the phase-locked regions has zero measure. Defining the fractal dimension D from the number $N(r)$ of steps larger than the scale r , $N(r) \sim r^{-D}$, it follows from the exponential decay of step widths with P that $D=0$.

Crossing the line l_1 from *B* into region *A* the widths of the steps grow from 0 in a way that abruptly changes the measure of phase-locked regions from zero on l_1 to completeness in *A*. Close to l_1 the steps grow linearly with the distance $dA = A_{\text{top}} - A_{\text{bot}}$. Since $1-\Lambda_+ \sim dA$, Eq. (13) gives, to first order,

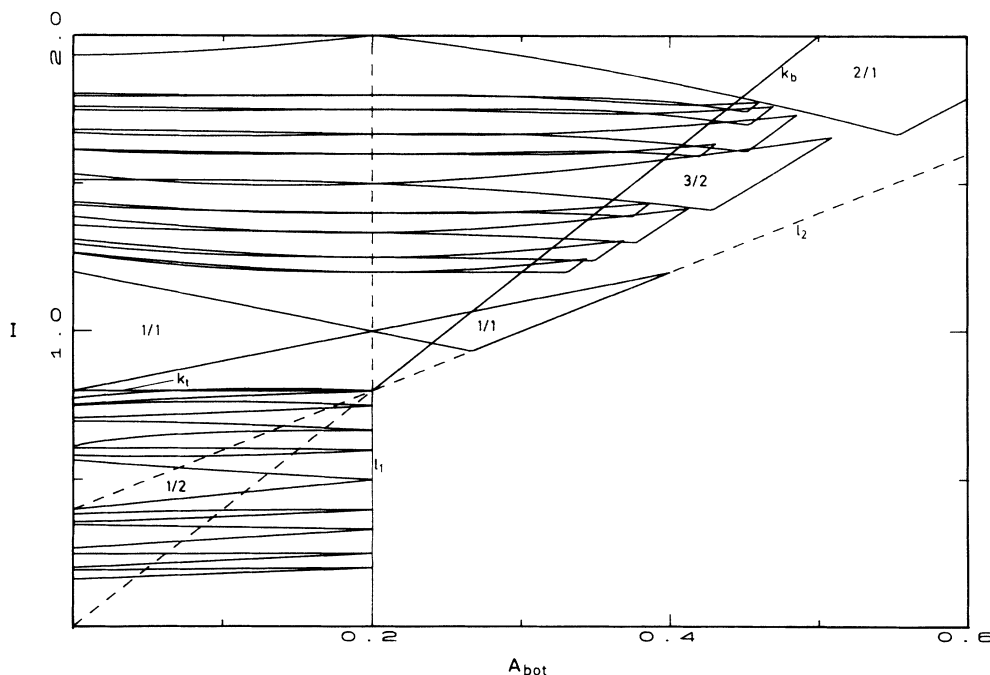


FIG. 4. Phase-locked regions in (I, A_{bot}) space for $A_{\text{top}}=0.2$. The largest regions are marked with their rotation number P/Q . Also the lines k_l, k_b, l_1 , and l_2 are shown.

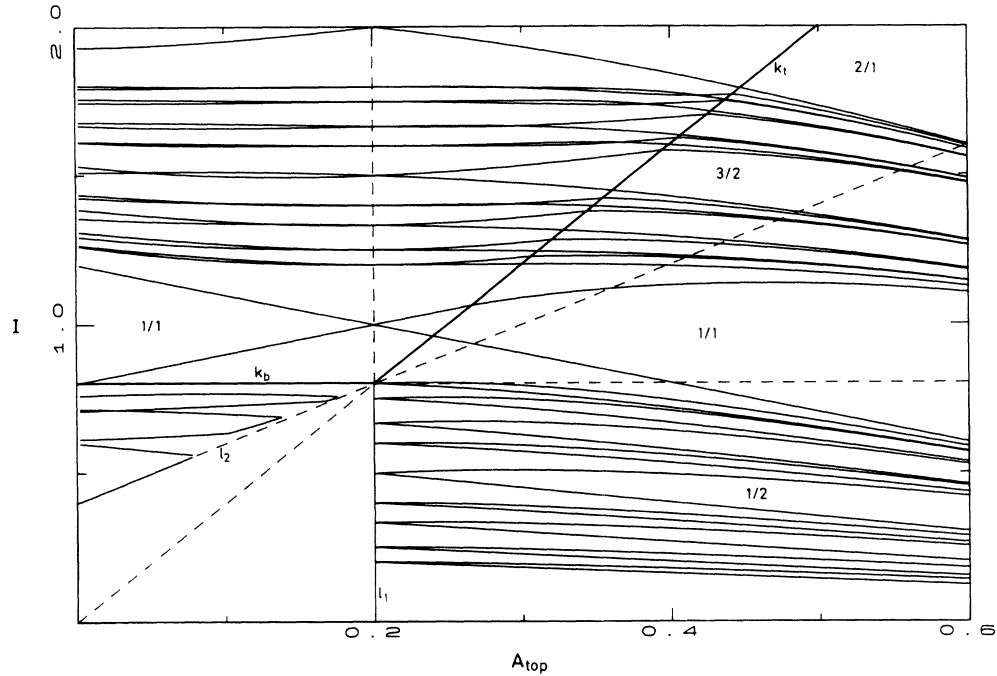


FIG. 5. Phase-locked regions in (I, A_{top}) space for $A_{bot}=0.2$. The largest regions are marked with their rotation number P/Q . Also the lines k_t, k_b, l_1 , and l_2 are shown.

$$\Delta \frac{1}{I}(P/Q) \sim \frac{1}{P} dA . \tag{18}$$

$$\Delta I(F_i/F_{i+1}) \sim \frac{1}{F_i} dA . \tag{20}$$

For small steps, $\Delta(1/I) \sim \Delta I/I^2$, and using that $I=P/Q$ on l_1 we have

$$\Delta I(P/Q) \sim \frac{P}{Q^2} dA . \tag{19}$$

By Eq. (19) we find in particular that the widths $\Delta I(1/Q)$ of the $1/Q$ steps are inversely proportional to Q^2 , while the widths $\Delta I(F_i/F_{i+1})$ of the steps for the Fibonacci sequence F_i/F_{i+1} ($F_0=1, F_1=1, F_{i+1}=F_i+F_{i-1}$) are inversely proportional to F_i :

Figure 8 shows $\ln[\Delta I(F_i/F_{i+1})]$ as function of $\ln(dA)$. For small values of dA , the curves are linear with a slope of 1, and separated by a distance $\ln(F_{i+1}/F_i)$, which for large i approaches the value $\ln[(\sqrt{5}+1)/2] \approx 0.4812$.

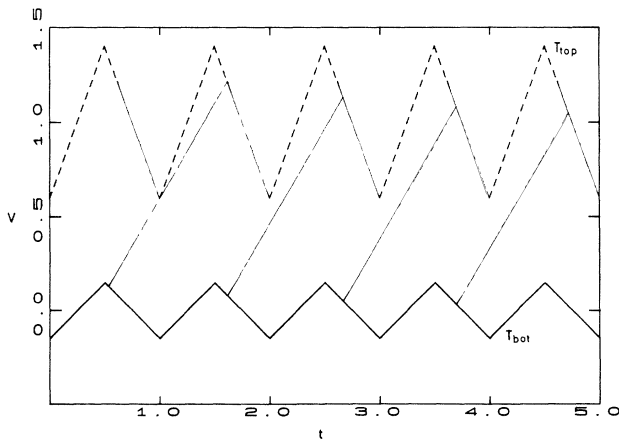


FIG. 6. Firings in the intervals $[n, n + \frac{1}{2}]$ cannot take place due to the shadowing effect from the intervals $[n + \frac{1}{2}, n + 1]$.

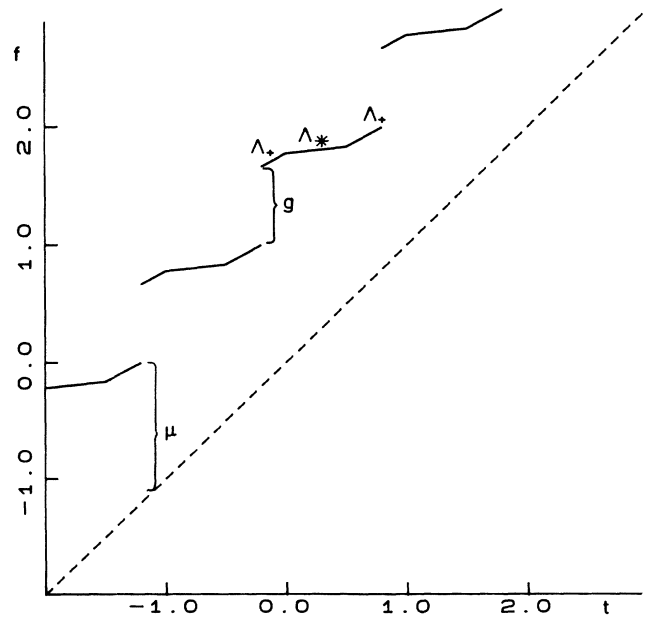


FIG. 7. The firing function $f(t)$ for parameters $I=0.6, A_{top}=0.3$, and $A_{bot}=0.1$ in region A.

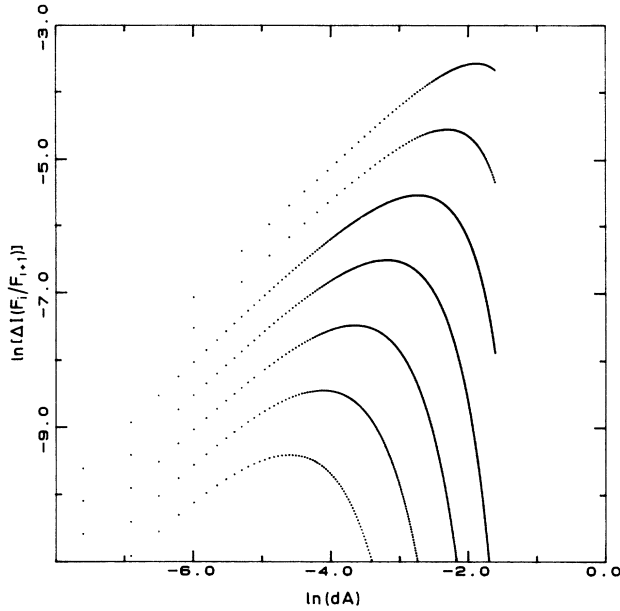


FIG. 8. A ln-ln plot of the widths $\Delta I(P/Q)$ of the steps for the Fibonacci sequence F_i/F_{i+1} as a function of the distance $dA = A_{\text{top}} - A_{\text{bot}}$ from l_1 for $A_{\text{top}} = 0.2$. From top to bottom the rotation number is $\frac{3}{5}$, $\frac{5}{8}$, $\frac{8}{13}$, $\frac{13}{21}$, $\frac{21}{34}$, $\frac{34}{55}$, and $\frac{55}{89}$.

However, the linear increase in step widths stops closer to l_1 as F_i increases. Such behavior is necessary in order for the phase-locked regions not to start overlapping.

When $\hat{A}_{\text{top}} < 1$ firings can take place at all times and we have divided this region into four ($C-F$) (Fig. 3). In the region D where $\hat{A}_{\text{top}} < 1$, $\hat{A}_{\text{bot}} < 1$, and $\hat{A}_{\text{bot}} > \hat{A}_{\text{top}}$, we have $\Lambda_+ > 1$ and $0 < \Lambda_- < 1$ making the existence of both quasiperiodic and phase-locked attractors possible. A periodic attractor on the lower (upper) edge I_l (I_u) of a step will fire at $\tau_0 = n + \frac{1}{2}$ ($\tau_0 = n$) where the modulation is maximum (minimum). When τ_0 crosses $n + \frac{1}{2}$ (n), the number P_+ increases by 1 while P_- decreases by 1, making the stability criterion Eq. (9) invalid. Starting on l_1 (where almost all attractors are quasiperiodic) and increasing \hat{A}_{bot} , phase-locked steps appear (Fig. 4). The phase-locked regions display distinct hourglass shapes with the step widths in some points decreasing to zero.⁹ Nonetheless, the total measure of the phase-locked regions continues to grow and the phase locking becomes complete on the line $k_b: \hat{A}_{\text{bot}} = 1$, where the increasing part of the lower threshold has a slope of I . Considering the inverse firing function f^{-1} , the arguments leading to Eq. (13) can be repeated. The step widths $\Delta(1/I)(P/Q)$ are obtained from Eq. (13) by substituting Λ_+^{-1} for Λ_+ . In particular, the fractal dimension along k_b is zero.

Inside region E where $\hat{A}_{\text{bot}} > 1$, $\hat{A}_{\text{top}} > 1$, and $\hat{A}_{\text{top}} + \hat{A}_{\text{bot}} < 2$, the phase-locked regions continue to grow near k_b causing them to overlap. Figure 9 shows two different attractors in the same point in parameter space on the $\frac{5}{3}$ step and $\frac{7}{4}$ step, respectively. As in region D , the upper edge I_u of a phase-locked region is given by $\tau_0 = n$. The lower edge I_l , on the other hand, is given by $\tau_0 = n + \frac{1}{2}$ only near k_b . Consider, for example, A_{top} fixed

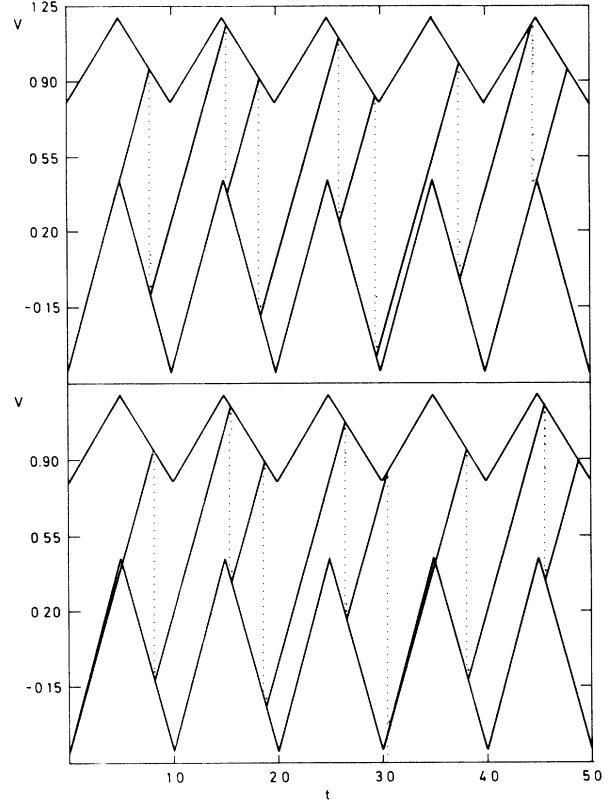


FIG. 9. Two different attractors with $R = \frac{5}{3}$ and $\frac{7}{4}$, respectively, in the same point $(I, A_{\text{bot}}, A_{\text{top}}) = (1.705, 0.45, 0.2)$ in region E .

(Fig. 4). While the upper edge I_u of a step increases in region E , the lower edge I_l only decreases until the stability is lost at $\tau_0 = n + \frac{1}{2}$, and a knee emerges. I_l then increases until it meets I_u , where the phase locking is lost. On the line $l_2: \hat{A}_{\text{bot}} + \hat{A}_{\text{top}} = 2$, Λ_- becomes -1 , and all phase-locked regions have vanished. By a simple calculation we find the edges of the $1/Q$ regions

$$I_u = (1 + A_{\text{bot}} - A_{\text{top}})/Q \quad \text{if } A_{\text{top}} < A_{\text{bot}} < A_{\text{bot}}^u, \quad (21)$$

$$I_l = \begin{cases} (1 - A_{\text{bot}} + A_{\text{top}})/Q & \text{if } A_{\text{top}} < A_{\text{bot}} < A_{\text{bot}}^l \\ 2(A_{\text{top}} + A_{\text{bot}}) & \text{if } A_{\text{bot}}^l < A_{\text{bot}} < A_{\text{bot}}^u \end{cases}, \quad (22)$$

where

$$A_{\text{bot}}^l = \frac{1 - (2Q - 1)A_{\text{top}}}{2Q + 1}, \quad (23)$$

$$A_{\text{bot}}^u = \frac{1 - (2Q + 1)A_{\text{top}}}{2Q - 1}.$$

We see that the $1/Q$ regions disappear exactly on the line l_2 . But this is not typical. Numerically, we find that the distance from k_b to where the P/Q region disappears decays exponentially with the numerator P with the same exponent $P \ln(\Lambda_+)$ as in Eq. (13). This is not unexpected

noting that both I_u and I_l , except for the knee, are approximately linear in region E .

In region F where $\hat{A}_{bot} > 1$, $\hat{A}_{top} < 1$, and $\hat{A}_{top} + \hat{A}_{bot} > 2$, we have $\Lambda_- < -1$ and $\Lambda_+ > 1$, and all attractors are chaotic. In region C where $\hat{A}_{bot} < 1$, $\hat{A}_{top} < 1$, and $\hat{A}_{bot} < \hat{A}_{top}$ the situation is the same as in region D , except that I_l now is found by $t_0 = n$, and I_u by $\tau_0 = n + \frac{1}{2}$. Both periodic and quasiperiodic attractors are present and the phase-locked regions are hourglass shaped.

In Fig. 10, V_n ($n = 501, 502, \dots, 1500$) is displayed as function of A_{bot} for $I = \frac{10}{9}$ and $A_{top} = 0.2$ (i.e., $\hat{A}_{top} < 1$). We observe quasiperiodic and phase-locked attractors in region D ($0.2 < A_{bot} < 0.277\dots$), phase-locked and chaotic attractors in region E ($0.277\dots < A_{bot} < 0.355\dots$), and the absence of attractors other than chaotic ones in region F ($A_{bot} > 0.355\dots$). Several periodic windows are clearly seen in region D as well as a degenerated bifurcation tree and its inverse in region E . The associated Liapunov exponent λ is given by

$$\lambda = \lim_{t \rightarrow \infty} \frac{1}{t} [N_-(t) \ln(|\Lambda_-|) + N_+(t) \ln(\Lambda_+)] , \quad (24)$$

where $N_-(t)$ and $N_+(t)$ are the numbers of firings at times less than t on the intervals $[n, n + \frac{1}{2}]$ and $[n + \frac{1}{2}, n + 1]$, respectively. Figure 11 shows (for the same parameters as in Fig. 10) the values of λ obtained from the time interval $[501, 1500]$. Chaotic motion is associated with a positive value of λ .

Consider now the Poincaré map, i.e., V_{n+1} as function of V_n , where V_n is taken to be $V_n = V(n + \frac{1}{4})$ to keep V_n in the unit interval $[0, 1]$. For simplicity, assume $R < 1$. In this case an attractor will fire 0 or 1 times during a

time period 1. The Poincaré map will consist of two branches, one below the diagonal $V_{n+1} = V_n$ and one above. A point (V_n, V_{n+1}) on the branch above the diagonal corresponds to a situation where no firing has taken place in the time interval $]n, n + 1[$. Due to the linear increase of V between firings, $V_{n+1} = V_n + I$, so this branch has a slope of 1. Likewise a point on the branch below the diagonal corresponds to a situation where the system has fired exactly once in the period $]n, n + 1[$. This branch is piecewise linear with a slope of Λ_- or Λ_+ , according to whether the firing took place in the interval $]n, n + \frac{1}{2}[$ or $]n + \frac{1}{2}, n + 1[$. The break points P_1 and P_2 are determined by firings at $t = n$ and $n + \frac{1}{2}$, respectively (Fig. 12),

$$P_1 = (1 + A_{top} - 3I/4, I/4 + A_{bot}) , \quad (25)$$

$$P_2 = (1 - A_{top} - I/4, 3I/4 - A_{bot}) . \quad (26)$$

Note that the V_n values do not depend on A_{bot} while the V_{n+1} values do not depend on A_{top} .

Assume first $\hat{A}_{top} < 1$ [Figs. 12(a)–12(e)]. Starting in region C the map is one to one with $\Lambda_- > 1$ and $0 < \Lambda_+ < 1$. Increasing A_{bot} , both slopes will approach 1 until they are exactly 1 on the line l_1 . In region D , $\Lambda_+ > 1$ is increasing, $0 < \Lambda_- < 1$ is decreasing, and the map is still one to one until the critical line k_b is reached where the slope Λ_- becomes zero, and P_1 and P_2 both have the V_{n+1} value $2A_{bot}$, at which the map is noninvertible. In the region E , Λ_- becomes negative while Λ_+ continues to grow. The map is now noninvertible in an interval and coexistence of trajectories with different rotation numbers, as well as chaotic trajectories is possible. Λ_- decreases further as A_{bot} is increased (the slope Λ_- is

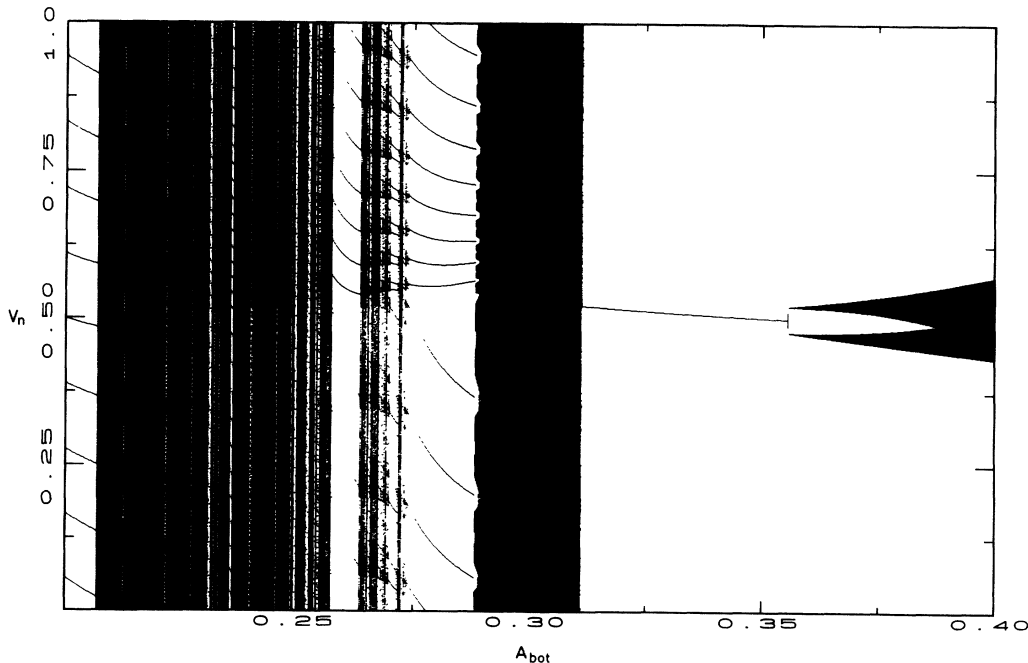


FIG. 10. V_n , $n = 501, 502, \dots, 1500$, as function of A_{bot} for $A_{top} = 0.2$ and $I = \frac{10}{9}$.

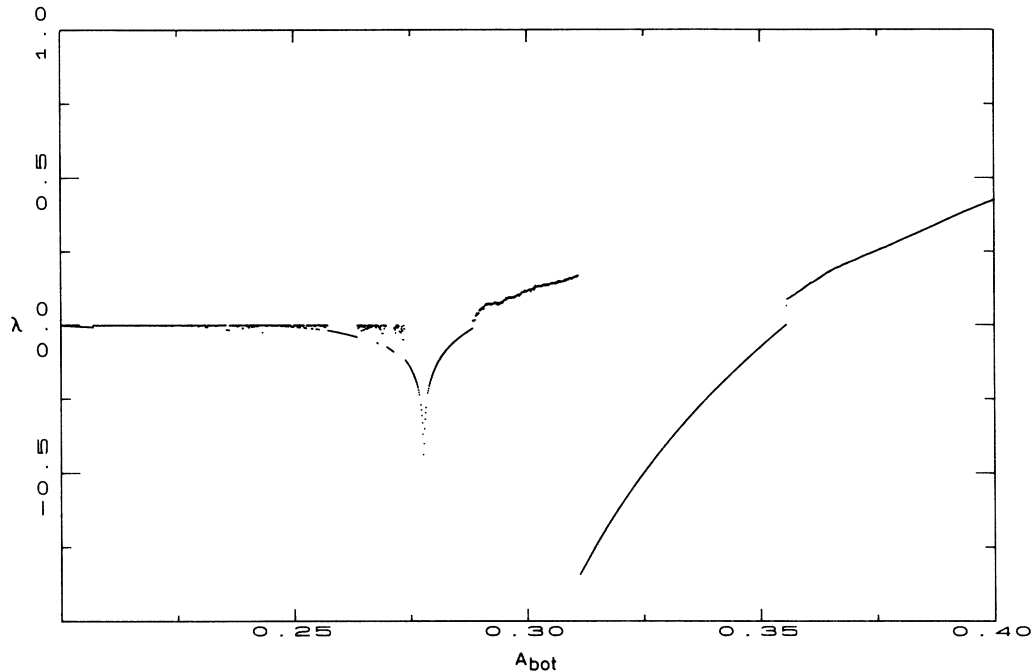


FIG. 11. Liapunov exponent λ as function of A_{bot} for the same parameters $A_{\text{top}}=0.2$ and $I=\frac{10}{9}$ as in Fig. 10. In both figures the first 500 time steps have been ignored for each value of A_{bot} to avoid the transient behavior.

-1 on the line separating regions E and F).

As mentioned above, the Poincaré map is one to one in region C [Fig. 12(a)]. Increasing A_{top} , the V_n coordinates of P_1 and P_2 are approaching each other, and Λ_- is diverging. On the line k_t [Fig. 12(f)] the V_n coordinates of P_1 and P_2 collapse, and a gap emerges in the lower branch of the Poincaré map at $V_n = 1 - 2A_{\text{top}}$. In region A [Fig. 12(g)] the V_n coordinate of P_1 exceeds that of P_2 and the Poincaré map is now apparently multivalued. However, the shadowing effect of the upper modulation opens a gap inaccessible for attractors in the Poincaré map, making it effectively single valued. The gap opens abruptly with a size $2(A_{\text{top}} - A_{\text{bot}})$ at the line k_t , and the gap size grows as the region A is penetrated. It is worth noting that the existence of one gap implies an infinity of inaccessible regions in the Poincaré map for an attractor.

In summary, we have treated a simple modulated integrate-and-fire system, and we have obtained analytical results for its phase diagram. In particular, we have identified the critical lines k_t and k_b , one associated with a nonchaotic transition to CPL, the other with the onset of chaos. Also a critical line l_1 exists which separates a CPL region and a chaotic region. In all cases, we have related the behavior to the Liapunov exponent and the specific form of the Poincaré map.

In the fixed A_{top} projection (Fig. 4), we notice that the transition at the line k_b is clearly seen as the edges of the phase-locked regions are nearly normal to this line. In contrast the edges are nearly parallel to the line k_t , and the transition on k_t is hard to observe. In Fig. 5 the situation is reversed. Here the edges of the phase-locked regions are nearly normal to k_t and nearly parallel to k_b .

Substituting the triangular modulation with a

sinusoidal $M(t) = \sin(2\pi t)$ only changes the details of the systems behavior—the overall structure of the parameter space is left unaltered. The parameter space will be divided into regions by critical lines $\hat{A}_{\text{bot}} = 1$ and $\hat{A}_{\text{top}} = 1$ where the normalized amplitudes now are $\hat{A}_{\text{bot}} = 2\pi A_{\text{bot}}/I$ and $\hat{A}_{\text{top}} = 2\pi A_{\text{top}}/I$. In region D the hourglass shapes will be replaced by monotonically growing phase-locked regions, but all attractors will still be quasiperiodic or periodic and the Poincaré map one to one. Again the measure of the phase-locked regions will grow from zero on $l_1: \hat{A}_{\text{bot}} = \hat{A}_{\text{top}}$ to completeness on k_b , where the fractal dimension is now $D=0.87$ and the Poincaré map (at irrational values of R) develops a *horizontal* inflection point. In region E the phase-locked regions start to overlap giving birth to the complicated scenario of chaotic attractors and periodic windows known from circle map studies.¹ Also on the line k_t we have CPL with fractal dimension $D=0.87$, but the Poincaré map has a *vertical* inflection point.⁵ In region A a gap is present in the Poincaré map and the phase locking is complete with fractal dimension $D=0$. Near k_t the gap size grows square-root-like with the distance from k_t .⁹ In the region B all attractors will be chaotic and again the line l_1 , where $R=I$, will separate this region from the CPL region A .

Let us briefly comment on the changes in the phase diagram when damping is added. Then the variable V asymptotically converges towards a constant value (Fig. 13), giving rise to a nonfiring region (zero-step) if this value is less than the minimum of the upper threshold. For clarity, consider the specific system with triangular modulation [Eqs. (2) and (3)] and the evolution between firings determined by

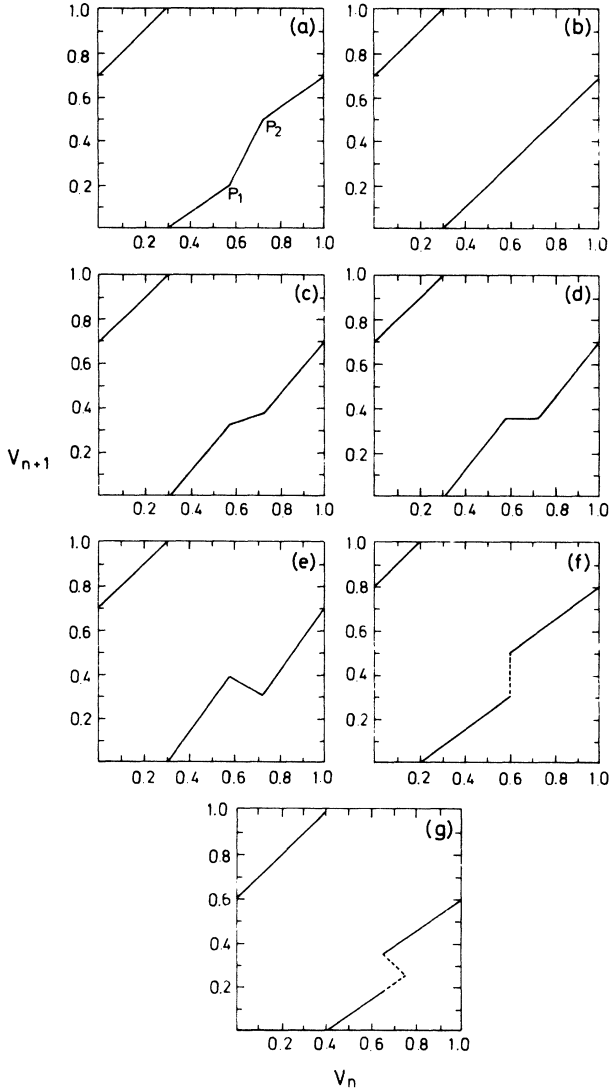


FIG. 12. Poincaré maps in the different regions in parameter space. In (a)–(e), $A_{\text{top}}=0.1$ and $I=0.7$, while in (f) and (g), $A_{\text{top}}=0.2$ and $A_{\text{bot}}=0.1$. (a) In region C with $A_{\text{bot}}=0.025$; (b) on line l_1 with $A_{\text{bot}}=0.1$; (c) in region D with $A_{\text{bot}}=0.15$; (d) on line k_b with $A_{\text{bot}}=0.175$; (e) in region E with $A_{\text{bot}}=0.22$; (f) on line k_t with $I=0.8$; (g) in region A with $I=0.6$.

$$\dot{V} = I - \Gamma V, \quad (27)$$

where the damping $\Gamma > 0$. The asymptotic value of V is I/Γ ($\dot{V}=0$), and the zero-step is therefore given by $I/\Gamma < 1 - A_{\text{top}}$. The critical lines k_b and k_t are determined by $V=4A_{\text{bot}}$, $V=A_{\text{bot}}$, and $\dot{V}=4A_{\text{top}}$,

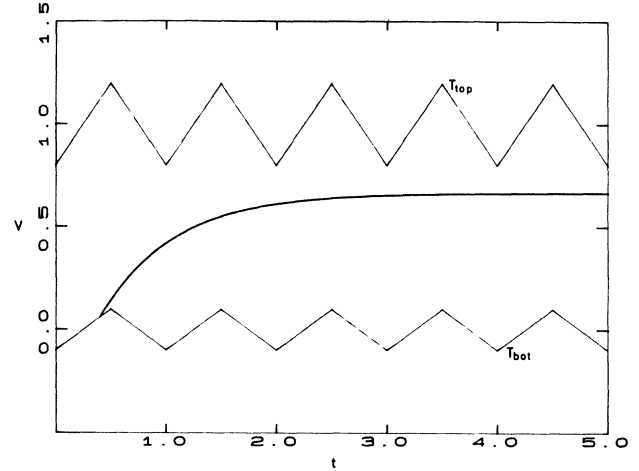


FIG. 13. A nonfiring trajectory converging towards a fixed point $V=2/3$ in the presence of damping. The parameters are $A_{\text{bot}}=0.1$, $A_{\text{top}}=0.2$, $I=1$, and $\Gamma=1.5$.

$V=1 + A_{\text{top}}$, respectively. This gives

$$k_b: \hat{A}_{\text{bot}} = \frac{1}{1 + \Gamma/4}, \quad (28)$$

$$k_t: \hat{A}_{\text{top}} = \frac{1 - \Gamma/I}{1 + \Gamma/4}. \quad (29)$$

The damping suppresses both critical lines in the reduced parameter space $(\hat{A}_{\text{bot}}, \hat{A}_{\text{top}})$, k_t more than k_b . Note that k_t now depends explicitly on the control parameter I . The curve l_1 separating the CPL region A and the region B where all attractors are chaotic is no longer a straight line, and $R < I$. However, l_1 still joins k_t and k_b in their mutual point of intersection.

We conclude the paper by commenting on the influence of relaxing the requirement of identical phases and frequencies. When relaxing the requirements on phases the only difference is found for regions B and F, which include phase-locked solutions except for the in-phase and antiphase situations. For different frequencies the system becomes more complex. In general, the frequencies are incommensurate, allowing, in addition to chaotic attractors, for two- and three-frequency quasiperiodicity. In spite of these complications, the regions in parameter space persist. The characterization summarized in Table I is still valid with the above-mentioned modifications if one substitutes periodic attractors with two-frequency quasiperiodic attractors, and quasiperiodic attractors with three-frequency quasiperiodic attractors.

¹See, e.g., M. H. Jensen, P. Bak, and T. Bohr, Phys. Rev. A **30**, 1960 (1984), and references therein.

²S. E. Brown, G. Mozurkewich, and G. Grüner, Phys. Rev. Lett. **52**, 2277 (1984).

³J. Maselko and H. L. Swinney, J. Chem. Phys. **85**, 6430 (1986).

⁴A. Cumming and P. S. Linsay, Phys. Rev. Lett. **59**, 1633 (1987).

⁵P. Alstrøm, B. Christiansen, and M. T. Levinsen, Phys. Rev. Lett. **61**, 1679 (1988).

⁶See, e.g., A. J. Diefenderfer, *Principles of Electronic Instrumentation* (Saunders, Philadelphia, 1972), p. 284.

⁷P. Alstrøm and M. T. Levinsen, Phys. Rev. B **40**, 4609 (1989).

⁸J. F. Fohlmeister, Kybernetik **13**, 104 (1973); P. Alstrøm and

M. T. Levinsen, Phys. Lett. A **138**, 127 (1988).

⁹P. Alstrøm, B. Christiansen, and M. T. Levinsen, Phys. Rev. B **41**, 1308 (1990).

¹⁰B. Christiansen and M. T. Levinsen (unpublished).

¹¹For the system to be properly defined we require $T_{\text{top}}(t) > T_{\text{bot}}(t)$, i.e., $1 + A_{\text{top}} > A_{\text{bot}}$ and $1 + A_{\text{bot}} > A_{\text{top}}$. Evidently we only consider nontrivial initial conditions (t_s, V_s) with $V_s < T_{\text{top}}(t_s)$.

¹²The lower edge $I_l(P/Q)$ will belong to the phase-locked region, $I_u(P/Q)$ will not.

¹³If $\hat{A}_{\text{bot}} \geq 1$, the *largest* value of μ for which $f(-\mu)=0$ is chosen.

¹⁴P. Alstrøm, Ph.D. thesis, Copenhagen, 1986; P. Alstrøm, Commun. Math. Phys. **104**, 581 (1986); E. Ding and J. Hemmer, J. Stat. Phys. **46**, 99 (1987).